ACS APPLIED ENERGY MATERIALS

Article

Cite This: ACS Appl. Energy Mater. 2019, 2, 5769−5776

www.acsaem.org

Cerium Phosphate as a Novel Cocatalyst Promoting $NiCo_2O_4$ Nanowire Arrays for Efficient and Robust Electrocatalytic Oxygen Evolution

Wei Gao,[†,‡,▽] Wangyan Gou,[†,▽] Yuanyuan Ma,[†] Renjie Wei,[§,∥] Johnny C. Ho,[*,§,∥,⊥] and Yongquan Qu[*,†,#]

[†]Center for Applied Chemical Research, Frontier Institute of Science and Technology, Xi'an Jiaotong University, Xi'an 710049, China

[‡]State Key Laboratory of Solidification Processing, Center for Nano Energy Materials, School of Materials Science and Engineering, Northwestern Polytechnical University and Shaanxi Joint Laboratory of Graphene (NPU), Xi'an 710072, P. R. China

[§]Department of Materials Science and Engineering and [⊥]State Key Laboratory of Terahertz and Millimeter Waves, City University of Hong Kong, 83 Tat Chee Avenue, Kowloon, Hong Kong

[∥]Shenzhen Research Institute, City University of Hong Kong, Shenzhen 518057, China

[#]Institute of Advanced Electrochemical Energy, Xi'an University of Technology, Xi'an, 710048, China

Supporting Information

ABSTRACT: Incorporating electrocatalysts with rare earth elements has attracted increasing attention in electrocatalysis because of its effective modulation of their chemical and electronic structures for enhanced catalytic hydrogen and oxygen evolution reactions. Herein, cerium phosphate ($CePO_4$) is demonstrated to be a novel cocatalyst that significantly enhances the OER performance of $NiCo_2O_4$ nanowire arrays on Ni foam. The high durability of OER performance over 1000 h and the low overpotential of 281 mV required to maintain a catalytic current density of 20 mA cm^{-2} can be attributed to the synergetic effect between $CePO_4$ and $NiCo_2O_4$. Explicitly, $CePO_4$ as a cocatalyst efficiently tunes the surface states of $NiCo_2O_4$ and facilitates water adsorption and the conversion of intermediates, leading to a substantial OER performance enhancement. All results exhibit the potential of integrating $CePO_4$ into $NiCo_2O_4$ to improve the water oxidation activity of $NiCo_2O_4$ and illustrate wide domains of application by combining rare earth elements into electrocatalysts.

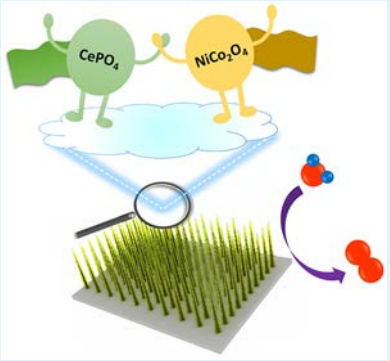

KEYWORDS: *electrocatalysis, oxygen evolution reaction, cerium, cocatalyst, $CePO_4$*

1. INTRODUCTION

In the past decade, the emission of greenhouse gases and toxic substances, such as carbon dioxide and nitrogen oxides, caused by using fossil fuels has invaded our environment. Since then, harvesting sustainable energy is widely considered to be a critical means to reduce pollution as well as to acquire clean energy. In general, water electrolysis is an important approach to generating high-purity hydrogen as an environmentally friendly fuel for vehicles and power stations and as a chemical raw material for industrial applications and also serves as a promising strategy for converting electricity obtained from renewable energy into storable energy resources.[1−3] Nonprecious transition metals are usually considered to be competitive catalyst candidates for overall water splitting because of their advantages in low cost and high abundance.[4−7] During the operation of electrochemical water splitting, the oxygen evolution reaction (OER) is an anodic half reaction, which is a complex process that takes place in either acid, neutral, or alkaline solutions. It involves a four-electron procedure with sluggish kinetics on the surfaces of electrodes and requires large overpotentials to initiate the catalytic reaction.[8,9] To promote this slow process, the rational design of electrode materials can facilitate the adsorption of active species, the conversion of intermediates, and the desorption of generated oxygen molecules. Many approaches, including the design of ultrathin two-dimensional materials, the intentional creation of defects and vacancies, the doping of foreign atoms, the coupling with conductive substrates, and building heterogeneous structures with oxygen-favored species, have been developed to accelerate the OER process.[10−24] In particular, anchoring cocatalysts on the catalytically active species is broadly regarded as an effective scheme for sensitizing and modulating the catalysts' activity.[25,26]

At the same time, because cobalt phosphate with the Co_4O_4 cubane structure was discovered to be a very efficient OER electrocatalyst in a neutral electrolyte,[27] great effort was

Received: May 6, 2019
Accepted: July 10, 2019
Published: July 10, 2019

DOI: 10.1021/acsaem.9b00903
ACS Appl. Energy Mater. 2019, 2, 5769−5776

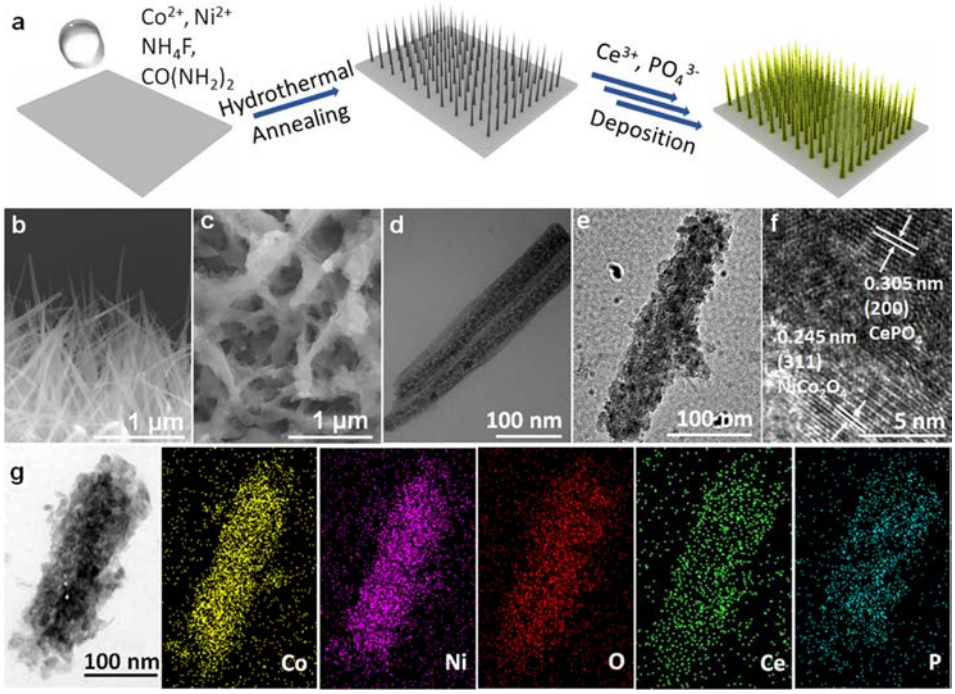

Figure 1. Characterizations of $NiCo_2O_4$ and $CePO_4/NiCo_2O_4$. (a) Scheme of the synthesis route of $CePO_4/NiCo_2O_4$ nanowire array catalysts. (b) SEM image of $NiCo_2O_4$ nanowires. (c) SEM image of $CePO_4/NiCo_2O_4$. (d) TEM image of $NiCo_2O_4$. (e) TEM image and (f) HRTEM image of $CePO_4/NiCo_2O_4$. (g) Elemental mapping images of $CePO_4/NiCo_2O_4$.

devoted to developing transition-metal-based phosphates into high-performance OER catalysts involving manganese, cobalt, nickel, and iron phosphates in either a neutral or alkaline medium.[28−37] Typically, the phosphate group as a proton acceptor plays an important role in OER by expediting the proton-coupled electron-transfer process between water and the environment.[27,28,38] Specifically, Yang et al. demonstrated that phosphate groups located on the perovskite surface could promote the proton transfer process with higher OER kinetics.[38] Furthermore, metal phosphates could also contribute to the locally distorted metal tetrahedral geometry, which favors the adsorption and oxidation of water molecules.[30] For instance, the distorted metal coordination geometry with the longer Co−O and Co−Co distances in cobalt diphosphate was found to significantly enhance the corresponding OER performance with the lower overpotentials required for specific current densities.[34]

Moreover, recent advances have also exhibited the promise and potential of integrating rare earth elements with electrocatalysts for the enhanced hydrogen evolution reaction, oxygen evolution reaction, oxygen reduction reaction, and other electrocatalytic reactions.[16,39−55] Among various rare earth elements, cerium (Ce) and its oxide (CeO_2) have attracted wide interest because of the good oxophilicity of Ce in modulating the electronic structures of the host catalysts[38] and the efficient conversion of intermediates to O_2 promoted by CeO_2 with the strong oxygen storage/release capacity in the OER process,[16,39,44,45] respectively. Moreover, cerium phosphate ($CePO_4$) has recently been proposed to be the catalyst for electrochemical oxygen reduction because of its contribution in providing more Ce^{3+} and oxygen vacancies.[49] Even though Ce-based materials are not very active for OER, they are shown to serve as excellent cocatalysts to enhance the OER performance of electrocatalysts.

Inspired by the above progress, herein we propose the idea of combining the advantages of both Ce and phosphate and demonstrate $CePO_4$ to be a novel cocatalyst to substantially improve the OER activity of $NiCo_2O_4$. By simply employing $NiCo_2O_4$ nanowire arrays directly fabricated on Ni foam as model OER catalysts, coating $CePO_4$ on the surface of $NiCo_2O_4$ nanowires can be readily achieved by a facile chemical deposition method. Importantly, a vast improvement in the OER catalytic activity of $CePO_4$-decorated $NiCo_2O_4$ nanowire arrays was observed with the much smaller overpotentials of 281 and 349 mV to realize current densities of 20 and 100 mA cm^{-2}, respectively, as compared to those of 325 and 383 mV for the undecorated counterparts. This OER performance enhancement is mostly attributed to the properly modulated surface states of electroactive Ni and Co sites as well as the benefits of integrating $CePO_4$ cocatalysts to facilitate the corresponding water adsorption and intermediate conversion during the water oxidation process.

2. EXPERIMENTAL SECTION

2.1. Preparation of $CePO_4/NiCo_2O_4$. $NiCo_2O_4$ nanowire arrays were prepared on Ni foam by a hydrothermal method followed by thermal annealing. To be specific, Ni foam with a size of 2 × 3 cm^2 was first cleaned successively in 10% HCl aqueous solution, deionized water, and ethanol with ultrasonication for 10 min, respectively, and then dried by blowing nitrogen gas. Then, the clean Ni foam was placed in the Teflon-lined stainless-steel autoclave filled with 30 mL of transparent solution containing 0.5 mmol $Ni(NO_3)_2{\cdot}6H_2O$, 1 mmol $Co(NO_3)_2{\cdot}6H_2O$, 2 mmol NH_4F, and 3 mmol urea. The hydrothermal process was performed in an electrical oven and kept at 120 °C for 6 h. After cooling to room temperature, the obtained precursor-coated Ni foam was washed with ethanol and deionized water alternatively for several cycles and then dried at 60 °C. Afterward, the precursors were annealed in air at 350 °C for 2 h with a temperature ramp of 5 °C/min to obtain $NiCo_2O_4$ nanowire arrays on Ni foam. To coat the $CePO_4$ layer, a piece (1 × 3 cm^2) of Ni foam

DOI: 10.1021/acsaem.9b00903
ACS Appl. Energy Mater. 2019, 2, 5769−5776

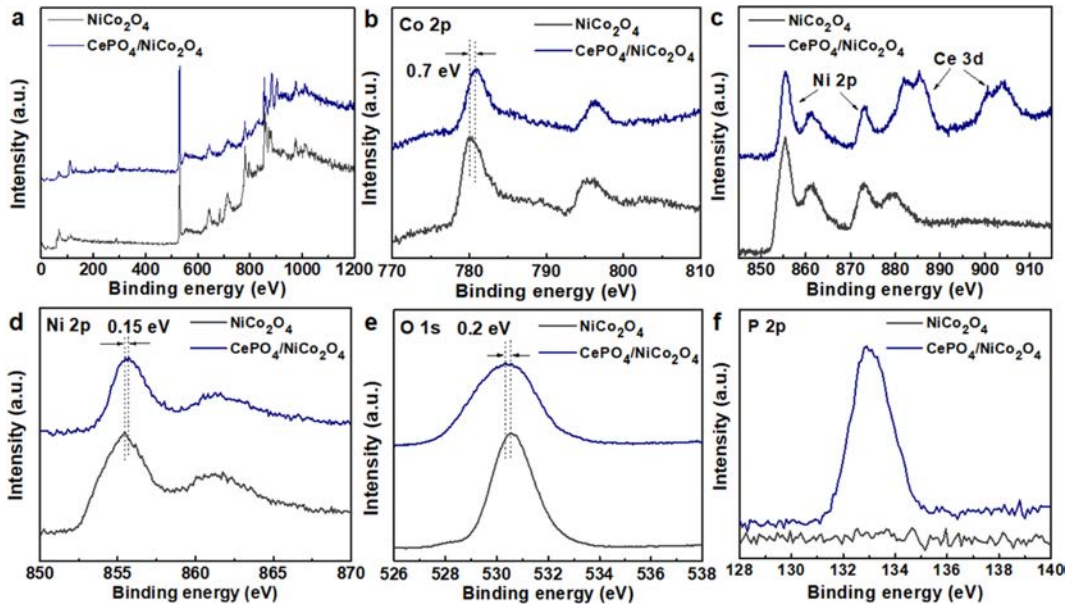

Figure 2. Typical XPS spectra of $NiCo_2O_4$ and $CePO_4/NiCo_2O_4$. (a) Full scan, (b) Co 2p, (c) Ni 2p and Ce 3d, (d) Ni 2p, (e) O 1s, and (f) P 2p.

supported with $NiCo_2O_4$ nanowires was immersed in 10 mL of 0.05 M $(NH_4)_2HPO_4{\cdot}2H_2O$ solution for 30 s and then 10 mL of 0.05 M $Ce(NO_3)_3{\cdot}6H_2O$ solution for another 30 s to finish one deposition cycle. The loading of $CePO_4$ on $NiCo_2O_4$ nanowires was dictated by the number of deposition cycles. Eventually, the obtained electrodes were blown dry with nitrogen gas, followed by drying at 60 °C overnight.

2.2. Preparation of $NiCo_2O_4$–Ce^{3+} and $NiCo_2O_4$–PO_4^{3-}. Ce^{3+}-functionalized $NiCo_2O_4$ and phosphate-ion-functionalized $NiCo_2O_4$ were prepared by immersing the as-synthesized nanowire arrays in 0.05 M $CeCl_3$ and K_3PO_4 solutions, respectively, and then dried at 60 °C overnight. A blank sample of $NiCo_2O_4$ was also treated in water with the same procedure.

2.3. Characterization. To evaluate the morphology of the obtained samples, scanning electron microscopy (SEM) images were collected with a Philips LX 30 FEG microscope with an accelerating voltage of 20 kV, while transmission electron microscopy (TEM) and high-resolution TEM (HR-TEM) images were obtained from a JEOL JEM-2100F microscope with an accelerating voltage of 200 kV. The energy-dispersive X-ray spectrum (EDS) was acquired from an Oxford Instruments and EDAX Inc. instrument in order to determine the composition and distribution of various elements of the fabricated samples. X-ray diffraction (XRD) patterns were also measured using a Rigaku powder X-ray diffractometer with Cu Kα radiation. X-ray photoelectron spectra (XPS) were collected from a ULVAC-PHI Inc. (model 5802) X-ray photoelectron spectrometer. The ratios of Ce to Co in various samples were measured by using PerkinElmer NexION 360D inductively coupled plasma–mass spectrometry (ICP–MS).

2.4. Electrochemical Measurements. All the electrochemical tests were performed with a Gamry G300 electrochemical workstation (Gamry Instruments, USA) using a three-electrode setup to measure the activity and stability of various samples, where the as-prepared samples on Ni foam, a Ag/AgCl (3 M KCl) electrode, and a graphite rod were employed as the working electrode, reference electrode, and counter electrode, respectively. Before testing, the active geometric areas of various samples immersed in electrolyte were defined by sealing with silicone rubber. The linear sweeping voltammetry (LSV) method was used with a scan rate of 5 mV/s in 1.0 M KOH solution to test the polarization curves at room temperature. The stability tests of electrocatalysts for OER were performed using the chronopotentiometry method with a fixed current density of 50 mA cm^{-2} and the chronoamperometry method with a fixed overpotential of 400 mV. The potential scale with respect to the reverse hydrogen electrode (RHE) was corrected by the Nernst equation, where $E_{vs\ RHE} = E_{vs\ Ag/AgCl\ (3\ M\ KCl)} + 0.0592 \times pH + 0.197$ (V). Electrochemical impedance spectroscopy (EIS) was also measured under a fixed overpotential of 400 mV with a frequency range of 100 kHz to 0.1 Hz. Also, because the electrochemically active surface area (ECSA) is proportional to the double-layer capacitance (C_{dl}), cyclic voltammetry (CV) curves with different scan rates were measured to calculate their intrinsic activity. All polarization curves were *iR* corrected unless otherwise mentioned.

3. RESULTS AND DISCUSSION

3.1. Fabrication and Characterization of $CePO_4/NiCo_2O_4$. As shown in Figure 1a, the $NiCo_2O_4$ nanowire arrays fabricated on Ni foam were first prepared by using a facile hydrothermal approach followed by annealing in air to obtain the metal oxide nanowires. $CePO_4$ was then used to decorate the nanowires through a repetitive wet chemical deposition method. Scanning electron microscopy (SEM) images in Figures 1b and S1a revealed the long and vertically aligned $NiCo_2O_4$ nanowires. After decorating with $CePO_4$ in three cycles, the obtained electrode displayed a hierarchical network structure with the features of individual $NiCo_2O_4$ nanowires wrapped and interconnected with $CePO_4$ nanoparticles (Figures 1c and S1b), suggesting the versatility and reliability of this facile chemical coating method. To further confirm the $CePO_4$ coating, X-ray diffraction (XRD) patterns of both as-synthesized $NiCo_2O_4$ nanowires and $CePO_4$-coated $NiCo_2O_4$ nanowires (named $CePO_4/NiCo_2O_4$) were collected (Figure S2). For the $NiCo_2O_4$ nanowire electrodes, the dominant peaks at 18.9, 31.1, 36.7, 38.4, 59.1, and 65.0° were indexed to the cubic structure of $NiCo_2O_4$ (PDF no. 20-0781). After the decoration of $CePO_4$, the new XRD peaks at 29.2 and 31.4° ascribed to the hexagonal $CePO_4$ phase (PDF no. 34-1380) appeared.

Next, $NiCo_2O_4$ and $CePO_4/NiCo_2O_4$ were characterized by transmission electron microscopy (TEM). Figure 1d exhibited the typical TEM image of $NiCo_2O_4$ nanowires with a diameter of tens of nanometers. Small $CePO_4$ nanoparticles were also confirmed to be deposited successfully on the $NiCo_2O_4$ nanowire surface (Figure 1e). Lattice fringes with interplanar

DOI: 10.1021/acsaem.9b00903
ACS Appl. Energy Mater. 2019, 2, 5769–5776

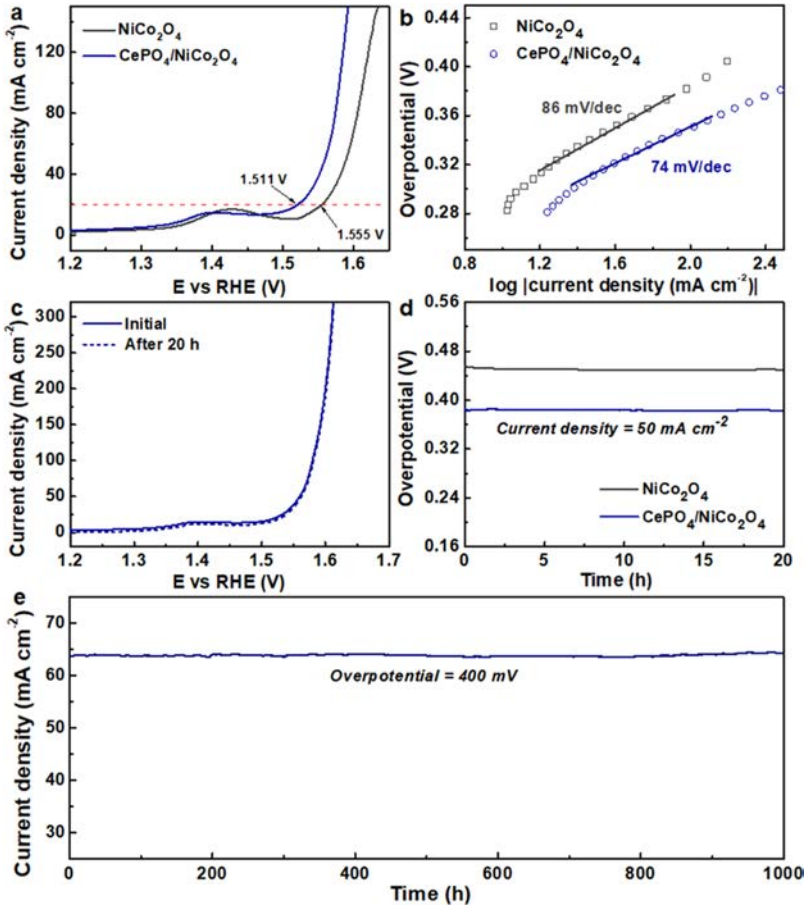

Figure 3. Electrocatalytic OER property of the $NiCo_2O_4$ and $CePO_4/NiCo_2O_4$ electrocatalysts at ~25 °C in 1.0 M KOH solution. (a) Polarization curves of $NiCo_2O_4$ and $CePO_4/NiCo_2O_4$ at a scan rate of 10 mV/s. (b) Tafel slopes of $NiCo_2O_4$ and $CePO_4/NiCo_2O_4$ derived from (a). (c) Polarization curves of $CePO_4/NiCo_2O_4$ before and after the stability test. (d) Stability test of $NiCo_2O_4$ and $CePO_4/NiCo_2O_4$ with a fixed current density of 50 mA cm^{-2} using the chronopotentiometry method without *iR* corrections. (e) Long-term stability evaluation of $CePO_4/NiCo_2O_4$ over 1000 h under an overpotential of 400 mV using the chronoamperometry method without *iR* corrections.

spacings of 0.245 and 0.305 nm were also observed in the HRTEM image, corresponding to the (311) plane of $NiCo_2O_4$ and the (200) plane of $CePO_4$, respectively, suggesting the existence of $CePO_4$ in $CePO_4/NiCo_2O_4$ electrodes (Figure 1f). The existence of Ce and P elements in $CePO_4/NiCo_2O_4$ was also confirmed by elemental mapping (Figure 1g) and X-ray energy-dispersive spectrum (EDS) analysis (Figure S3). Therefore, all of the analyses can evidently confirm the formation of $CePO_4$ on $NiCo_2O_4$ nanowire arrays.

In addition, the surface chemical states of both $NiCo_2O_4$ and $CePO_4/NiCo_2O_4$ electrocatalysts were analyzed by X-ray photoelectron spectroscopy (XPS, Figure 2a). For Co species, the peaks at ~780 and 796 eV were ascribed to the oxidized Co species, while those located at ~787 and 803 eV were assigned to the satellite peaks of oxidized Co species (Figure 2b).[17,56] It is noted that the Co $2p_{3/2}$ peak in $CePO_4/NiCo_2O_4$ showed a significant upshift of 0.7 eV in the binding energy when compared to that in $NiCo_2O_4$, indicating a more positively charged state of Co species in $CePO_4/NiCo_2O_4$. Figure 2c showed the Ni 2p spectrum of $NiCo_2O_4$ as well as Ni 2p and Ce 3d spectra of $CePO_4/NiCo_2O_4$, revealing the presence of Ce in $CePO_4/NiCo_2O_4$. Also, the Ni $2p_{3/2}$ spectra illustrated the oxidized Ni species with main peaks at about 855.5 eV and satellite peaks at about 861 eV for both $NiCo_2O_4$ and $CePO_4/NiCo_2O_4$ (Figure 2d).[57] A similar upshift in the binding energy of Ni 2p of $CePO_4/NiCo_2O_4$ was also observed with a value of 0.15 eV as compared to that in $NiCo_2O_4$. Meanwhile, the O 1s spectrum of $CePO_4/NiCo_2O_4$ exhibited an apparent downshift of about 0.2 eV in the binding energy as contrasted with that of $NiCo_2O_4$ (Figure 2e). The P 2p spectrum with the peak located at 133 eV was assigned to the phosphate group with P−O bonding in $CePO_4/NiCo_2O_4$,[31] while there is no signal for the phosphorus element observed for $NiCo_2O_4$ (Figure 2f). Therefore, the XPS data clearly verified the existence of $CePO_4$ for the $CePO_4/NiCo_2O_4$ sample and suggested the properly modulated surface chemical states of $NiCo_2O_4$ by $CePO_4$. In particular, the upshifts in the binding energies for Ni and Co and the downshift for O suggest the strong interaction between $CePO_4$ and $NiCo_2O_4$ to promote Ni and Co with high oxidation states and O with electron-rich states, which would facilitate the OER process.[58,59]

3.2. OER Performance of $CePO_4/NiCo_2O_4$. The electrochemical OER process was recorded in 1.0 M KOH using a three-electrode setup to determine the catalytic performance of both $NiCo_2O_4$ and $CePO_4/NiCo_2O_4$. Initially, different loadings of $CePO_4$ on the $CePO_4/NiCo_2O_4$ catalysts were evaluated through this chemical deposition with varied cycles. Inductively coupled plasma−mass spectrometry (ICP−MS) was employed to determine the loading amount of $CePO_4$ in terms of the ratio of Ce/(Ce + Co). As shown in Figure S4, all $CePO_4/NiCo_2O_4$ electrodes performed better than the

DOI: 10.1021/acsaem.9b00903
ACS Appl. Energy Mater. 2019, 2, 5769−5776

$NiCo_2O_4$ sample with the lower overpotentials to drive specific current densities. However, when the loading of $CePO_4$ was too high, it would require larger overpotentials resulting from the blockage of active sites of $NiCo_2O_4$ with the excessive $CePO_4$. Therefore, the loading of $CePO_4$ was optimized with three deposition cycles with a Ce/(Ce + Co) ratio of 0.15 in the $CePO_4/NiCo_2O_4$ electrocatalyst, which was utilized for all subsequent electrocatalytic OER studies in this work. As extracted from the polarization curves (Figure 3a), the $NiCo_2O_4$ nanowire arrays required an overpotential of 325 mV to obtain a current density of 20 mA cm^{-2}. In contrast, the required overpotential was reduced to only 281 mV for $CePO_4/NiCo_2O_4$. As a control, commercial RuO_2 on Ni foam demanded an overpotential of 300 mV to afford a current density of 20 mA cm^{-2} (Figure S5). At a larger current density of 100 mA cm^{-2}, an overpotential of 349 mV was demanded for $CePO_4/NiCo_2O_4$, also being much smaller than that for $NiCo_2O_4$ of 383 mV. Moreover, $NiCo_2O_4$ delivered a relatively large Tafel slope of 86 mV/dec, while $CePO_4/NiCo_2O_4$ exhibited a smaller value of 74 mV/dec (Figure 3b). To further evaluate the difference in their catalytic activities, current densities of these two different electrodes at various overpotentials are presented in Figure S6. Specifically, the current density at an overpotential of 375 mV was determined to be 238.6 mA cm^{-2} for $CePO_4/NiCo_2O_4$, which was 2.9 times higher than that (82.2 mA cm^{-2}) for $NiCo_2O_4$. Therefore, the performance of $CePO_4/NiCo_2O_4$ is demonstrated to be much better than that of $NiCo_2O_4$ and is also the best among many state-of-the-art nonprecious OER electrocatalysts (Table S1), indicating the extraordinary enhancement effect of $CePO_4$ as a cocatalyst.

To shed light on the actual catalytic active surface area of these electrocatalysts, the double-layer capacitance (C_{dl}), proportional to the electrochemically active surface area (ECSA), was directly measured to evaluate the quantity of the interface active site by ECSA = C_{dl}/C_s. C_s is the specific capacitance, which has a typical value of 0.04 mF cm^{-2} in the basic solution.[60] The plots of non-Faradaic capacitive current densities versus different scan rates were also obtained from cyclic voltammetry (CV) curves (Figure S7a,b) for $NiCo_2O_4$ and $CePO_4/NiCo_2O_4$. As given in Figure S7c, the C_{dl} values of $NiCo_2O_4$ and $CePO_4/NiCo_2O_4$ were determined to be 16.7 and 32.6 mF cm^{-2}, respectively, suggesting that more active sites of $CePO_4/NiCo_2O_4$ were exposed in electrolyte as a result of the surface decoration with $CePO_4$. Similarly, Figure S7d exhibited better catalytic activity for $CePO_4/NiCo_2O_4$ as compared to that of $NiCo_2O_4$ for OER based on the evaluation of their polarization curves with normalization to ECSA, which again demonstrated the enhanced intrinsic activity at each catalytic active site of $NiCo_2O_4$ after surface decoration with $CePO_4$. In addition, Nyquist plots derived from electrochemical impedance spectroscopy (EIS) also showed the better conductivity of $CePO_4/NiCo_2O_4$ as compared to that of $NiCo_2O_4$ resulting from the smaller charge-transfer resistance and improved electrolyte/electrode interface (Figure S8). Thus, the high performance of $CePO_4/NiCo_2O_4$ makes it a possible electrode candidate for not only electrocatalytic water oxidation but also photoelectrocatalytic water splitting with the cooperation of good light absorbers.[61]

The durability of both $CePO_4/NiCo_2O_4$ catalysts was also investigated in 1.0 M KOH using the cyclic voltammetry method for 2000 cycles (Figure S9) and the chronopotentiometry method with a fixed current density of 50 mA cm^{-2} without *iR* corrections (Figure 3c,d). For $CePO_4/NiCo_2O_4$, the polarization curves before and after 2000 CV cycles were almost the same, as accompanied by the preservation of morphology, as well as Ce and P elements (Figure S10). For both samples of $CePO_4/NiCo_2O_4$, small fluctuations were observed for overpotentials required to maintain the fixed current density during the 20 h test. The required overpotential of ~450 mV for $NiCo_2O_4$ was much larger than that for $CePO_4/NiCo_2O_4$ (~380 mV), indicating the better OER activity in the presence of $CePO_4$. For $CePO_4/NiCo_2O_4$, the polarization curve after the stability test almost overlapped with the initial curve, again confirming the excellent stability of the electrocatalyst (Figure 3c). Moreover, the $CePO_4/NiCo_2O_4$ electrodes also exhibited good activity and durability at a higher working temperature of 50 °C as illustrated in Figure S11. Impressively, an overpotential of 325 mV was needed only to afford a current density of 100 mA cm^{-2}, whereas high stability is witnessed during its 20 h chronopotentiometry test at 50 °C. To further assess the durability of $CePO_4/NiCo_2O_4$, a long-term stability test was performed under an overpotential of 400 mV for 1000 h. Excitingly, there is not any significant deterioration for the current density of ~64 mA cm^{-2} from the initial to the end of this test, illustrating the exceptional robustness of $CePO_4/NiCo_2O_4$ (Figure 3e). Because of the stable and conductive support of the Ni foam, $NiCo_2O_4$ nanowires as the robust host electrocatalysts are aligned on Ni foam for OER and play key roles in the good durability, which is also witnessed by the chronopotentiometry test with a fixed current density of 50 mA cm^{-2} as exhibited in Figure 3d. Moreover, the good cohesion of $CePO_4$ on $NiCo_2O_4$ and the chemical stability (Figure S10) of $CePO_4$ under alkaline conditions contributed to the improvement in activity for $NiCo_2O_4$ during such a long test. Therefore, the structural features and the combination of $CePO_4$ with $NiCo_2O_4$/Ni foam led to good stability for this 1000 h OER test.

3.3. Discussion. By all means, using $CePO_4$ to decorate $NiCo_2O_4$ nanowire arrays is herein demonstrated to be a reliable approach to promoting the OER catalytic activity of $NiCo_2O_4$, but the role of $CePO_4$ needs to be clarified. In this case, $CePO_4$ alone (Figure S12) was loaded onto the glassy carbon electrode at a density of 0.56 mg/cm^2, which exhibited negligible OER activity in 1.0 M KOH (Figure S12d), indicating that $CePO_4$ was inactive for OER. Loading $CePO_4$ onto Ni foam via the same method could somehow improve the activity of Ni foam for OER (Figure S13). Thus, it is logically inferred that $CePO_4$ would serve as a cocatalyst to facilitate the OER performance of electroactive catalysts instead of functioning as electroactive species.

As reported in the literature, phosphate groups with good hydrophilicity can promote the uptake of oxygen-involving intermediates to favor water adsorption,[31] working as a proton acceptor to facilitate the oxidation of metals on the surface as active sites[29] and to accelerate the proton-transfer kinetics of M−OH and M−OOH deprotonation processes, lowering the energy barrier for intermediate formation by tuning the electronic structure of host electrocatalysts.[38] Furthermore, Ce-based species and Ce-dopants are also known as efficient cocatalysts for improving the oxygen-involving electrochemical reactions because of the good oxophilicity of Ce[41] and large oxygen storage capacity of CeO_2 as oxygen buffers.[16,39,46] Thus, thorough investigations were then performed to obtain further insight into evaluating the roles of Ce^{3+} and phosphate

DOI: 10.1021/acsaem.9b00903
ACS Appl. Energy Mater. 2019, 2, 5769−5776

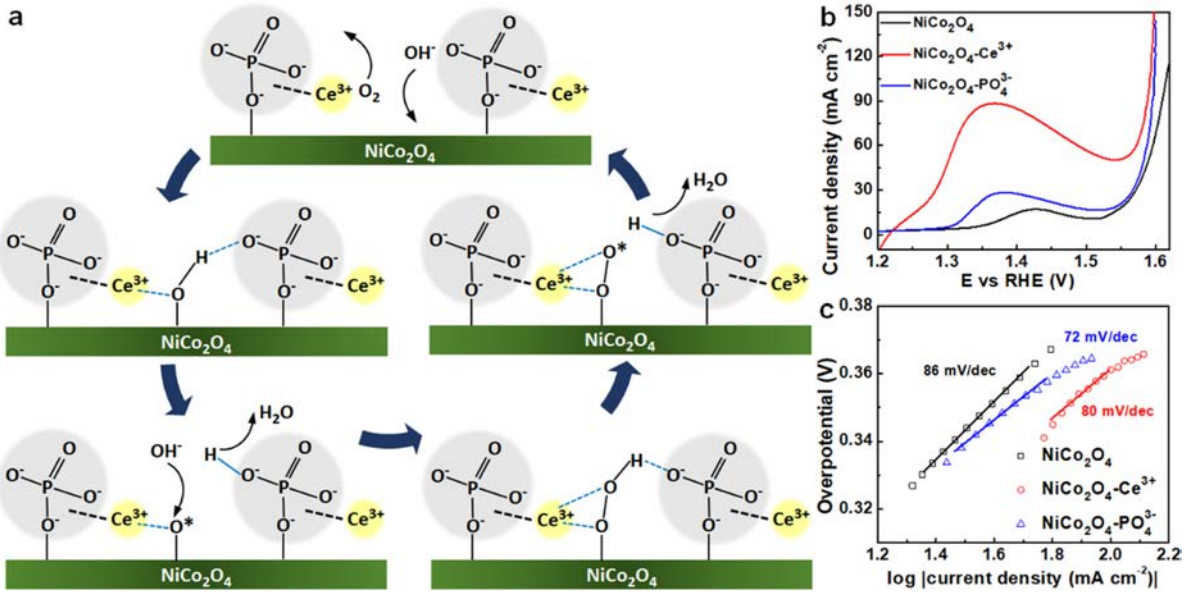

Figure 4. (a) Proposed OER mechanism of $CePO_4$ as the cocatalyst. (b) Polarization curves and (c) Tafel slope compilations of $NiCo_2O_4$, $NiCo_2O_4$–Ce^{3+}, and $NiCo_2O_4$–PO_4^{3-}, respectively.

groups. Explicitly, $NiCo_2O_4$ on Ni foam functionalized by the respective Ce^{3+} and phosphate ions (assigned as $NiCo_2O_4$–Ce^{3+} and $NiCo_2O_4$–PO_4^{3-}, respectively) were prepared and characterized by XPS, as described in Figure S14.

Both $NiCo_2O_4$–Ce^{3+} and $NiCo_2O_4$–PO_4^{3-} electrodes were observed to deliver lower overpotentials and smaller Tafel slopes than those of $NiCo_2O_4$ alone (Figure 4b), suggesting the positive enhancement induced by both Ce^{3+} and phosphate ions. In the case of $NiCo_2O_4$–Ce^{3+}, Ce^{3+} ions were transformed to $Ce(OH)_3$ and deposited onto the surface of $NiCo_2O_4$ nanowires in an alkaline medium, which can absorb more water molecules and OH^- ions to promote the oxidation of Ni^{2+} to Ni^{3+} as demonstrated by the significantly improved peaks at a potential of about 1.36 V (vs RHE). The excellent oxophilic property of $Ce(OH)_3$ can expedite the adsorption of hydroxide ions and the formation and release of oxygen molecules, being analogous to the effects of the Ce-dopant and CeO_2 as buffers for oxygen-containing species.[16,41,46] Similarly, Ce species in $CePO_4$ could also promote the adsorption of oxygen-containing species and work as the buffer for the formation and release of molecular oxygen for $CePO_4$/$NiCo_2O_4$, leading to enhanced OER activity as compared to that for $NiCo_2O_4$. As for $NiCo_2O_4$–PO_4^{3-}, the small Tafel slope (72 mV/dec, Figure 4c) suggests that after introducing PO_4^{3-} as the proton acceptor, the deprotonation process of M–OOH to form M–OO* is accelerated, while their good hydrophilicity can promote the adsorption of hydroxide ions and water molecules, being consistent with previous reports.[31,38] Thus, utilizing $CePO_4$ as a combination of Ce^{3+} and phosphate would have a unique advantages in the improved proton-transfer kinetics caused by PO_4^{3-} as well as the faster transformation of the M–OO* intermediates into oxygen with the help of Ce, which leads to better activity for the OER process. Besides, an OER mechanism for $CePO_4$/$NiCo_2O_4$ is proposed through a conventional four-electron process with $NiCo_2O_4$ as the catalytically active species and $CePO_4$ as the cocatalyst (Figure 4a), in which phosphate promotes the deprotonation of M–OH and M–OOH in different steps and Ce aids the formation and stability of M–OO* together with its turnover to O_2.

4. CONCLUSIONS

$CePO_4$ is recognized as a novel cocatalyst to significantly improve the OER activity of $NiCo_2O_4$. The enhancement in the activity of $NiCo_2O_4$ after decorating with $CePO_4$ can be ascribed to the following reasons. (1) The properly modulated surface chemical states of Ni and Co with high oxidation states as well as O with electron-rich states would facilitate OER as a result of the interaction between $CePO_4$ and $NiCo_2O_4$. (2) The acceleration of proton transfer kinetics and good hydrophilicity of phosphate groups as proton acceptors would facilitate the adsorption and deprotonation of intermediates.[27,29,38] (3) The good oxophilicity of Ce^{3+} in $CePO_4$ would benefit the formation of intermediates and their subsequent conversion and release of oxygen molecules.[41] Furthermore, $CePO_4$/$NiCo_2O_4$ also presents impressive stability for long time, >1000 h, with a large current density of ~64 mA cm^{-2}. All of these advantages would lead to the enhanced activity of $NiCo_2O_4$ decorated with $CePO_4$ as the superb electrocatalyst for OER processes.

■ ASSOCIATED CONTENT

Supporting Information

The Supporting Information is available free of charge on the ACS Publications website at DOI: 10.1021/acsaem.9b00903.

Additional characterization and analysis of data for the electrocatalysts and comparison of OER performance (PDF)

■ AUTHOR INFORMATION

Corresponding Authors

*E-mail: johnnyho@cityu.edu.hk.

*E-mail: yongquan@mail.xjtu.edu.cn.

ORCID

Wei Gao: 0000-0001-7606-7402

Renjie Wei: 0000-0002-0459-7196

DOI: 10.1021/acsaem.9b00903
ACS Appl. Energy Mater. 2019, 2, 5769–5776

Johnny C. Ho: 0000-0003-3000-8794
Yongquan Qu: 0000-0002-6202-1929

Author Contributions

[∇]These authors contributed equally to this work.

Notes

The authors declare no competing financial interest.

■ ACKNOWLEDGMENTS

The authors acknowledge the financial support from the National 1000-Plan program, National Natural Science Foundation of China (grant 21872109), the Fundamental Research Funds for the Central Universities (3102019QD0406), the Science Technology and Innovation Committee of Shenzhen Municipality (grant JCYJ20170818095520778), and the Environment and Conservation Fund of Hong Kong SAR, China (ECF 2016-85). Y.Q. also acknowledges support from the Cyrus Tang Foundation through the Tang Scholar Program.

■ REFERENCES

(1) Zou, X. X.; Zhang, Y. Noble Metal-Free Hydrogen Evolution Catalysts for Water Splitting. *Chem. Soc. Rev.* **2015**, *44*, 5148−5180.
(2) Seh, Z. W.; Kibsgaard, J.; Dickens, C. F.; Chorkendorff, I.; Nørskov, J. K.; Jaramillo, T. F. Combining Theory and Experiment in Electrocatalysis: Insights into Materials Design. *Science* **2017**, *355*, No. eaad4998.
(3) Roger, I.; Shipman, M. A.; Symes, M. D. Earth-Abundant Catalysts for Electrochemical and Photoelectrochemical Water Splitting. *Nat. Rev. Chem.* **2017**, *1*, 0003.
(4) Alarawi, A.; Ramalingam, V.; Fu, H.-C.; Varadhan, P.; Yang, R.; He, J.-H. Enhanced Photoelectrochemical Hydrogen Production Efficiency of MoS_2-Si Heterojunction. *Opt. Express* **2019**, *27*, A352−A363.
(5) Gao, W.; Gou, W.; Zhou, X.; Ho, J. C.; Ma, Y.; Qu, Y. Amine-Modulated/Engineered Interfaces of NiMo Electrocatalysts for Improved Hydrogen Evolution Reaction in Alkaline Solutions. *ACS Appl. Mater. Interfaces* **2018**, *10*, 1728−1733.
(6) Manikandan, A.; Ilango, P. R.; Chen, C.-W.; Wang, Y.-C.; Shih, Y.-C.; Lee, L.; Wang, Z. M.; Ko, H.; Chueh, Y.-L. A Superior Dye Adsorbent towards the Hydrogen Evolution Reaction Combining Active Sites and Phase-Engineering of (1T/2H) MoS_2/α-MoO_3 Hybrid Heterostructured Nanoflowers. *J. Mater. Chem. A* **2018**, *6*, 15320−15329.
(7) Suen, N.-T.; Huang, S.-F.; Quan, Q.; Zhang, N.; Xu, Y.-J.; Chen, H. M. Electrocatalysis for the Oxygen Evolution Reaction: Recent Development and Future Perspectives. *Chem. Soc. Rev.* **2017**, *46*, 337−365.
(8) Reier, T.; Nong, H. N.; Teschner, D.; Schlögl, R.; Strasser, P. Electrocatalytic Oxygen Evolution Reaction in Acidic Environments-Reaction Mechanisms and Catalysts. *Adv. Energy Mater.* **2017**, *7*, 1601275.
(9) Han, L.; Dong, S. J.; Wang, E. K. Transition-Metal (Co, Ni, and Fe)-Based Electrocatalysts for the Water Oxidation Reaction. *Adv. Mater.* **2016**, *28*, 9266−9291.
(10) Wang, G. M.; Yang, Y.; Han, D. D.; Li, Y. Oxygen Defective Metal Oxides for Energy Conversion and Storage. *Nano Today* **2017**, *13*, 23−29.
(11) Zhao, X.; Li, X.; Yan, Y.; Xing, Y.; Lu, S.; Zhao, L.; Zhou, S.; Peng, Z.; Zeng, J. Electrical and Structural Engineering of Cobalt Selenide Nanosheets by Mn Modulation for Efficient Oxygen Evolution. *Appl. Catal., B* **2018**, *236*, 569−575.
(12) Liu, Y. W.; Cheng, H.; Lyu, M. J.; Fan, S. J.; Liu, Q. H.; Zhang, W. S.; Zhi, Y. D.; Wang, C. M.; Xiao, C.; Wei, S. Q.; Ye, B. J.; Xie, Y. Low Overpotential in Vacancy-Rich Ultrathin $CoSe_2$ Nanosheets for Water Oxidation. *J. Am. Chem. Soc.* **2014**, *136*, 15670−15675.
(13) Liu, R.; Wang, Y.; Liu, D.; Zou, Y.; Wang, S. Water-Plasma-Enabled Exfoliation of Ultrathin Layered Double Hydroxide Nanosheets with Multivacancies for Water Oxidation. *Adv. Mater.* **2017**, *29*, 1701546.
(14) Zhao, Y. X.; Chang, C.; Teng, F.; Zhao, Y. F.; Chen, G. B.; Shi, R.; Waterhouse, G. I. N.; Huang, W. F.; Zhang, T. R. Defect-Engineered Ultrathin δ-MnO_2 Nanosheet Arrays as Bifunctional Electrodes for Efficient Overall Water Splitting. *Adv. Energy Mater.* **2017**, *7*, 1700005.
(15) Feng, J.-X.; Ye, S.-H.; Xu, H.; Tong, Y.-X.; Li, G.-R. Design and Synthesis of FeOOH/CeO_2 heterolayered nanotube electrocatalysts for the Oxygen Evolution Reaction. *Adv. Mater.* **2016**, *28*, 4698−4703.
(16) Feng, J.-X.; Xu, H.; Dong, Y.-T.; Ye, S.-H.; Tong, Y.-X.; Li, G.-R. FeOOH/Co/FeOOH Hybrid Nanotube Arrays as High-Performance Electrocatalysts for the Oxygen Evolution Reaction. *Angew. Chem.* **2016**, *128*, 3758−3762.
(17) Wang, S.; He, P.; Jia, L.; He, M.; Zhang, T.; Dong, F.; Liu, M.; Liu, H.; Zhang, Y.; Li, C.; Gao, J.; Bian, L. Nanocoral-Like Composite of Nickel Selenide Nanoparticles Anchored on Two-Dimensional Multi-Layered Graphitic Carbon Nitride: A Highly Efficient Electrocatalyst for Oxygen Evolution Reaction. *Appl. Catal., B* **2019**, *243*, 463−469.
(18) Cai, Z.; Bu, X.; Wang, P.; Ho, J. C.; Yang, J.; Wang, X. Recent advances in Layered Double Hydroxide Electrocatalysts for the Oxygen Evolution Reaction. *J. Mater. Chem. A* **2019**, *7*, 5069−5089.
(19) Qiu, B.; Cai, L.; Wang, Y.; Ma, S.; Tsang, Y. H.; Chai, Y. Accelerated Oxygen Evolution Kinetics on Nickel-Iron Diselenide Nanotubes by Modulating Electronic Structure. *Mater. Today Energy* **2019**, *11*, 89−96.
(20) Wei, R.; Fang, M.; Dong, G.; Lan, C.; Shu, L.; Zhang, H.; Bu, X.; Ho, J. C. High-Index Faceted Porous Co_3O_4 nanosheets with Oxygen Vacancies for Highly Efficient Water Oxidation. *ACS Appl. Mater. Interfaces* **2018**, *10*, 7079−7086.
(21) Prabu, M.; Ketpang, K.; Shanmugam, S. Hierarchical nanostructured $NiCo_2O_4$ as an Efficient Bifunctional Non-Precious Metal Catalyst for Rechargeable Zinc-Air Batteries. *Nanoscale* **2014**, *6*, 3173−3181.
(22) Sivanantham, A.; Ganesan, P.; Shanmugam, S. Hierarchical $NiCo_2S_4$ Nanowire Arrays Supported on Ni foam: an Efficient and Durable Bifunctional Electrocatalyst for Oxygen And Hydrogen Evolution Reactions. *Adv. Funct. Mater.* **2016**, *26*, 4661−4672.
(23) Sivanantham, A.; Ganesan, P.; Estevez, L.; McGrail, B. P.; Motkuri, R. K.; Shanmugam, S. A Stable Graphitic, Nanocarbon-Encapsulated, Cobalt-Rich Core-Shell Electrocatalyst as an Oxygen Electrode in a Water Electrolyzer. *Adv. Energy Mater.* **2018**, *8*, 1702838.
(24) Yu, J. Y.; Zhou, W. J.; Xiong, T. L.; Wang, A. L.; Chen, S. W.; Chu, B. L. Enhanced Electrocatalytic Activity of Co@N-doped Carbon Nanotubes by Ultrasmall Defect-Rich TiO_2 Nanoparticles for Hydrogen Evolution Reaction. *Nano Res.* **2017**, *10*, 2599−2609.
(25) Zhang, J. F.; Liu, J. Y.; Xi, L. F.; Yu, Y. F.; Chen, N.; Sun, S. H.; Wang, W. C.; Lange, K. M.; Zhang, B. Single-Atom Au/NiFe layered Double Hydroxide Electrocatalyst: Probing the Origin of Activity for Oxygen Evolution Reaction. *J. Am. Chem. Soc.* **2018**, *140*, 3876−3879.
(26) Kanan, M. W.; Nocera, D. G. In Situ Formation of An Oxygen-Evolving Catalyst in Neutral Water Containing Phosphate and Co^{2+}. *Science* **2008**, *321*, 1072−1075.
(27) Guo, R.; Lai, X.; Huang, J.; Du, X.; Yan, Y.; Sun, Y.; Zou, G.; Xiong, J. Phosphate-Based Electrocatalysts for Water Splitting: Recent Progress. *ChemElectroChem* **2018**, *5*, 3822−3834.
(28) Jin, K.; Park, J.; Lee, J.; Yang, K. D.; Pradhan, G. K.; Sim, U.; Jeong, D.; Jang, H. L.; Park, S.; Kim, K.; Sung, N.-K.; Kim, S. H.; Han, S.; Nam, K. T. Hydrated Manganese(II) Phosphate $(Mn_3(PO_4)_2 \cdot 3H_2O)$ as A Water Oxidation Catalyst. *J. Am. Chem. Soc.* **2014**, *136*, 7435−7443.
(29) Kim, H.; Park, J.; Park, I.; Jin, K.; Jerng, S. E.; Kim, S. H.; Nam, K. T.; Kang, K. Coordination Tuning of Cobalt Phosphates towards Efficient Water Oxidation Catalyst. *Nat. Commun.* **2015**, *6*, 8253.

DOI: 10.1021/acsaem.9b00903
ACS Appl. Energy Mater. 2019, 2, 5769−5776

(30) Li, Y.; Zhao, C. Iron-Doped Nickel Phosphate as Synergistic Electrocatalyst for Water Oxidation. *Chem. Mater.* **2016**, *28*, 5659−5666.
(31) Xie, L.; Zhang, R.; Cui, L.; Liu, D.; Hao, S.; Ma, Y.; Du, G.; Asiri, A. M.; Sun, X. High-Performance Electrolytic Oxygen Evolution in Neutral Media Catalyzed by a Cobalt Phosphate Nanoarray. *Angew. Chem., Int. Ed.* **2017**, *56*, 1064−1068.
(32) Zhong, D.; Liu, L.; Li, D.; Wei, C.; Wang, Q.; Hao, G.; Zhao, Q.; Li, J. Facile and Fast Fabrication of Iron-Phosphate Supported on Nickel Foam as a Highly Efficient and Stable Oxygen Evolution Catalyst. *J. Mater. Chem. A* **2017**, *5*, 18627−18633.
(33) Zhou, T.; Du, Y.; Wang, D.; Yin, S.; Tu, W.; Chen, Z.; Borgna, A.; Xu, R. Phosphonate-Based Metal-Organic Framework Derived Co-P-C Hybrid as an efficient Electrocatalyst for Oxygen Evolution Reaction. *ACS Catal.* **2017**, *7*, 6000−6007.
(34) Yang, L.; Guo, Z.; Huang, J.; Xi, Y.; Gao, R.; Su, G.; Wang, W.; Cao, L.; Dong, B. Vertical Growth of 2D Amorphous $FePO_4$ Nanosheet on Ni foam: Outer and Inner Structural Design for Superior Water Splitting. *Adv. Mater.* **2017**, *29*, 1704574.
(35) Liu, B.; Peng, H.-Q.; Ho, C.-N.; Xue, H.; Wu, S.; Ng, T.-W.; Lee, C.-S.; Zhang, W. Mesoporous Nanosheet Networked Hybrids of Cobalt Oxide and Cobalt Phosphate for Efficient Electrochemical and Photoelectrochemical Oxygen Evolution. *Small* **2017**, *13*, 1701875.
(36) Chang, J.; Lv, Q.; Li, G.; Ge, J.; Liu, C.; Xing, W. Core-Shell Structured $Ni_{12}P_5/Ni_3(PO_4)_2$ Hollow Spheres as Bifunctional and Efficient Electrocatalysts for overall Water Electrolysis. *Appl. Catal., B* **2017**, *204*, 486−496.
(37) Yang, C.; Laberty-Robert, C.; Batuk, D.; Cibin, G.; Chadwick, A. V.; Pimenta, V.; Yin, W.; Zhang, L.; Tarascon, J.-M.; Grimaud, A. Phosphate Ion Functionalization of Perovskite Surfaces for enhanced Oxygen Evolution Reaction. *J. Phys. Chem. Lett.* **2017**, *8*, 3466−3472.
(38) Zheng, Y.-R.; Gao, M.-R.; Gao, Q.; Li, H.-H.; Xu, J.; Wu, Z.-Y.; Yu, S.-H. An Efficient $CeO_2/CoSe_2$ Nanobelt Composite for Electrochemical Water Oxidation. *Small* **2015**, *11*, 182−188.
(39) Liu, K.; Huang, X.; Wang, H.; Li, F.; Tang, Y.; Li, J.; Shao, M. Co_3O_4-CeO_2/C as a Highly Active Electrocatalyst for Oxygen Reduction Reaction in Al-Air Batteries. *ACS Appl. Mater. Interfaces* **2016**, *8*, 34422−34430.
(40) Ng, J. W. D.; García-Melchor, M.; Bajdich, M.; Chakthranont, P.; Kirk, C.; Vojvodic, A.; Jaramillo, T. F. Gold-Supported Cerium-Doped NiO_x Catalysts for Water Oxidation. *Nat. Energy* **2016**, *1*, 16053.
(41) Dong, Z.-W.; Liu, J.-Y.; Liu, W.-C.; Wang, L.; Cui, R.-C.; Luo, H.-L.; Guo, X.-L.; Zheng, S.-Z.; Qiao, X.-W. Du; Yang, J. Modest Oxygen-Defective Amorphous Manganese-Based Nanoparticle Mullite with Superior Overall Electrocatalytic Performance for Oxygen Reduction Reaction. *Small* **2017**, *13*, 1603903.
(42) Gao, W.; Yan, M.; Cheung, H.-Y.; Xia, Z.; Zhou, X.; Qin, Y.; Wong, C.-Y.; Ho, J. C.; Chang, C.-R.; Qu, Y. Modulating Electronic Structure of CoP Electrocatalysts towards Enhanced Hydrogen Evolution by Ce Chemical Doping in Both Acidic and Basic Media. *Nano Energy* **2017**, *38*, 290−296.
(43) Obata, K.; Takanabe, K. A permselective CeO_x Coating to Improve the Stability of Oxygen Evolution Electrocatalysts. *Angew. Chem.* **2018**, *130*, 1632−1636.
(44) Li, D.-J.; Gu, Z.-G.; Zhang, W.; Kang, Y.; Zhang, J. Epitaxial Encapsulation of Homodispersed CeO_2 in a Cobalt-Porphyrin Network Derived Thin Film for the Highly Efficient Oxygen Evolution Reaction. *J. Mater. Chem. A* **2017**, *5*, 20126−20130.
(45) Gao, W.; Xia, Z.; Cao, F.; Ho, J. C.; Jiang, Z.; Qu, Y. Comprehensive Understanding of the Spatial Configurations of CeO_2 in NiO for the Electrocatalytic Oxygen Evolution Reaction: Embedded or Surface-Loaded. *Adv. Funct. Mater.* **2018**, *28*, 1706056.
(46) Wang, X.; Yang, Y.; Diao, L.; Tang, Y.; He, F.; Liu, E.; He, C.; Shi, C.; Li, J.; Sha, J.; Ji, S.; Zhang, P.; Ma, L.; Zhao, N. CeO_x-Decorated NiFe-Layered Double Hydroxide for Efficient Alkaline Hydrogen Evolution by Oxygen Vacancy Engineering. *ACS Appl. Mater. Interfaces* **2018**, *10*, 35145−35153.
(47) Sivanantham, A.; Ganesan, P.; Shanmugam, S. A Synergistic Effect of Co and CeO_2 in Nitrogen-Doped Carbon Nanostructure for the Enhanced Oxygen Electrode Activity and Stability. *Appl. Catal., B* **2018**, *237*, 1148−1159.
(48) Yu, Y.; He, B.; Liao, Y.; Yu, X.; Mu, Z.; Xing, Y.; Xing, S. Preparation of Hollow $CeO_2/CePO_4$ with Nitrogen and Phosphorus Co-Doped Carbon Shells for Enhanced Oxygen Reduction Reaction Catalytic Activity. *ChemElectroChem* **2018**, *5*, 793−798.
(49) Gao, W.; Wen, D.; Ho, J. C.; Qu, Y. Incorporation of Rare Earth Elements with Transition Metal-Based Materials for Electrocatalysis: A Review for Recent Progress. *Mater. Today Chem.* **2019**, *12*, 266−281.
(50) Liu, Y.; Ma, C.; Zhang, Q.; Wang, W.; Pan, P.; Gu, L.; Xu, D.; Bao, J.; Dai, Z. 2D Electron Gas and Vacancy Induced High Oxygen Evolution Performances for Advanced Co_3O_4/Ceo_2 Nanohybrids. *Adv. Mater.* **2019**, *31*, 1900062.
(51) Wang, W.; Chen, J.-Q.; Tao, Y.-R.; Zhu, S.-N.; Zhang, Y.-X.; Wu, X.-C. Flowerlike Ag-Supported Ce-Doped Mn_3O_4 Nanosheet Heterostructure for a Highly Efficient Oxygen Reduction Reaction: Role of Metal Oxides in Ag Surface States. *ACS Catal.* **2019**, *9*, 3498−3510.
(52) Sultana, S.; Mansigh, S.; Parida, K. M. Phosphide Protected FeS_2 Anchored Oxygen Defect Oriented Ceo_2 ns Based Ternary Hybrid for Electrocatalytic and Photocatalytic N_2 Reduction to NH_3. *J. Mater. Chem. A* **2019**, *7*, 9145−9153.
(53) Xu, S.; Lv, C.; He, T.; Huang, Z.; Zhang, C. Amorphous Film of Cerium Doped Cobalt Oxide as a Highly Efficient Electrocatalyst for Oxygen Evolution Reaction. *J. Mater. Chem. A* **2019**, *7*, 7526−7532.
(54) Zhang, S.; Zhao, C.; Liu, Y.; Li, W.; Wang, J.; Wang, G.; Zhang, Y.; Zhang, H.; Zhao, H. Cu Doping in CeO_2 to Form Multiple Oxygen Vacancies for Dramatically Enhanced Ambient N_2 Reduction Performance. *Chem. Commun.* **2019**, *55*, 2952−2955.
(55) Liu, W.; Liu, H.; Dang, L.; Zhang, H.; Liu, X.; Yang, B.; Li, Z.; Zhang, X.; Lei, L.; Jin, S. Amorphous Cobalt-Iron Hydroxide Nanosheet Electrocatalyst for Efficient Electrochemical and Photo-Electrochemical Oxygen Evolution. *Adv. Funct. Mater.* **2017**, *27*, 1603904.
(56) Zhang, Y.; Ouyang, B.; Xu, J.; Chen, S.; Rawat, R. S.; Fan, H. J. 3D Porous Hierarchical Nickel-Molybdenum Nitrides Synthesized by RF Plasma as Highly Active and Stable Hydrogen-Evolution-Reaction Electrocatalysts. *Adv. Energy Mater.* **2016**, *6*, 1600221.
(57) Yeo, B. S.; Bell, A. T. Enhanced Activity of Gold-Supported Cobalt Oxide for the Electrochemical Evolution of Oxygen. *J. Am. Chem. Soc.* **2011**, *133*, 5587−5593.
(58) Zhu, C.; Guo, J.; Liu, L.; Wang, Y. Du; Qiao, S.-Z. Two-Dimensional Metal-Organic Frameworks with High Oxidation States for Efficient Electrocatalytic Urea Oxidation. *Chem. Commun.* **2017**, *53*, 10906−10909.
(59) Mccrory, C. C. L.; Jung, S.; Peters, J. C.; Jaramillo, T. F. Benchmarking Heterogeneous Electrocatalysts for the Oxygen Evolution Reaction. *J. Am. Chem. Soc.* **2013**, *135*, 16977−16987.
(60) Fu, H.-C.; Ramalingam, V.; Kim, H.; Lin, C.-H.; Fang, X.; Alshareef, H. N.; He, J.-H. MXene-contacted silicon solar cells with 11.5% efficiency. *Adv. Energy Mater.* **2019**, *9*, 1900180.
(61) Wang, H.-P.; Periyanagounder, D.; Li, A.-C.; He, J.-H. Fabrication of silicon hierarchical structures for solar cell applications. *IEEE Access* **2019**, *7*, 19395−19400.

DOI: 10.1021/acsaem.9b00903
ACS Appl. Energy Mater. 2019, 2, 5769−5776